Temperature-Dependent Energy Thresholds for Ion-Stimulated Defect Formation in Solids

Z. Wang and E. G. Seebauer*

Department of Chemical Engineering, University of Illinois, Urbana, Illinois 61801, USA

(Received 16 February 2005; published 30 June 2005)

Recent simulations and experiments have hinted that the solid temperature may affect the dynamics of defect formation when the energies of bombarding ions fall below about 100 eV. The present work offers direct experimental confirmation of this phenomenon through measurements of the energy thresholds for ion-enhanced surface diffusion of indium on silicon and germanium, where transport rates depend upon surface defect formation. Such temperature-dependent energy thresholds may offer a new means for modulating sputtering and defect formation in a variety of ion processing applications.

DOI: 10.1103/PhysRevLett.95.015501 PACS numbers: 61.80.Jh, 34.50.Dy, 61.82.Fk, 68.35.Fx

Defect formation by bombarding ions plays a key role in determining the properties of materials in applications such as plasma enhanced deposition, reactive ion etching, ion beam-assisted deposition, and ion implantation. Adjustment of the solid temperature during ion exposure sometimes affects the results; such phenomena have been well studied in the context of plasma etching [1–3], ion implantation [4–6], and beam-assisted deposition [7]. Higher temperatures are typically thought to enhance self-annealing and other thermally stimulated processes, rather than the ion-solid interactions themselves. However, measurements of beam-assisted deposition [8–12] and surface diffusion [13,14] have hinted that temperature may directly affect the dynamics of defect formation when ion energies fall below about 100 eV.

None of the experiments has yielded a conclusive explanation, but recent molecular dynamics simulations [15] suggest that energy thresholds decrease strongly (> 0.1 eV/K) as temperature increases. The physical picture offered by the simulations was not entirely clear, however, and lacked direct experimental confirmation. The present work offers a clearer picture, together with experimental confirmation of the primary simulation results through measurements of the energy thresholds for ion-enhanced surface diffusion of indium on silicon and germanium, where transport rates depend upon defect formation at or near the surface.

Surface diffusion was measured in ultrahigh vacuum via optical second harmonic microscopy [16,17]. This method directly images the micrometer-scale evolution of a one-dimensional submonolayer step concentration profile that is created with a molecular beam and retractable mask. Illumination of the profile with a pulsed laser generates second harmonic light in reflection, whose (small) yield varies with adsorbate concentration and therefore with position on the surface. Independent calibration of yield vs concentration via Auger electron spectroscopy permits direct conversion of raw second harmonic images into concentration profiles. Straightforward Boltzmann-Matano analysis then provides the diffusivity D.

We have used this microscopy to measure thermal diffusion of indium on Si(111) [18–20] and Ge(111) [21] as well as ion-influenced surface diffusion of Ge on Si(111) [13,14]. We chose indium as the adsorbate for the present work because indium diffuses fairly quickly on both Si and Ge and therefore offers good precision for the energy threshold measurements. The basic methodology has been described previously [13,14], except that the present experiments employed a new custom ion source capable of providing a higher flux ($\sim 2\times$) and a smaller energy spread ($\sim 4\times$). Separate experiments with retarding field optics placed in front of the surface provided precise flux and energy calibrations. The total energy spread of the beam increased linearly with acceleration voltage from 1.5 eV at 15 V acceleration to 5 eV at 65 V. Experiments were performed on atomically clean p-Si(111) (B-doped, 0.01 Ω cm) and n-Ge(111) (As-doped, 10 Ω cm). Indium diffusion on Si(111) exhibits no coverage dependence [18], and initial coverage was set at 0.5 monolayer (ML) in all experiments. Indium diffusion on Ge(111) does exhibit coverage dependence above 0.1 ML, so the coverage was set at 0.1 ML to minimize this complication. For both

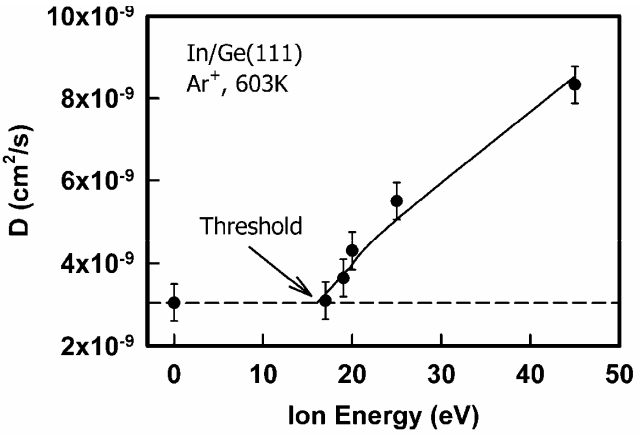

FIG. 1. Energy dependence of D for indium on Ge(111) during Ar^+ bombardment. The dashed line represents the thermal value. Threshold energy for the ion-induced increase lies at 16 ± 1 eV.

surfaces, ions of Ar^+ impinged at 60° off normal incidence with a constant flux of 5×10^{12} ions/cm^2 s.

Figure 1 shows typical data for the variation of D with Ar^+ ion energy E for Ge(111). Data for Si(111) followed a very similar pattern. The results show that ion-influenced surface diffusion is not restricted to Ge/Si(111), the lone case reported up to now [13,14]. There exists no *a priori* theory for the proper mathematical form to fit the data, so we used the phenomenological square-root dependence $D = D_{\text{thermal}} + A(E^{1/2} - E_{\text{thres}}{}^{1/2})$, where A and the threshold energy E_{thres} are fitting parameters. This form was chosen based on its satisfactory fit, its well-documented use for ion sputtering [22–25], and its success in fitting simulation data for ion-induced defect formation [15].

Figure 2 shows Arrhenius plots of the indium diffusivity on Si(111) for bombardment at several energies, along with data in the absence of bombardment. Even with ion bombardment, D exhibits conventional Arrhenius behavior in temperature T, with an activation energy E_{diff} and a preexponential factor D_0. Least-squares fitting of all the data sets yielded an average $E_{\text{diff}} = 1.65$ eV, with a standard deviation of 0.03 eV. Even this small standard deviation propagates into fairly large (factor of 2) variations in D_0, however, which is the main quantity affected by ion energy. Hence, Fig. 2 shows the data fitted with the constraint that $E_{\text{diff}} = 1.65$ eV. The corresponding preexponential factors vary by an order of magnitude, from the thermal value of 2.8×10^2 cm^2/s to 2.4×10^3 cm^2/s at an ion energy of 65 eV. Indium on Ge(111) exhibits similar behavior, with $E_{\text{diff}} = 1.02 \pm 0.02$ eV regardless of ion energy. The preexponential factors obtained using $E_{\text{diff}} = 1.02$ eV increase by a factor of 3 from the thermal value of 1.1 cm^2/s to 3.3 cm^2/s at 65 eV.

Figure 3 shows that for both Si and Ge, the threshold energy E_{thres} decreases significantly as T increases. The following phenomenological relation describes the data quite well:

$$E_{\text{thres}} = E_{\text{tot}} - \sigma kT, \tag{1}$$

where E_{tot} and σ denote constants and k is Boltzmann's constant. The constants for Si(111) are $\sigma = 1200 \pm 200$ and $E_{\text{tot}} = 107 \pm 14$ eV. For Ge(111), the corresponding numbers are $\sigma = 1440 \pm 140$ and $E_{\text{tot}} = 93 \pm 8$ eV.

The present experiments measure diffusion over a micrometer length scale, so that transport depends upon not only the rate of hopping diffusion but also the concentration of mobile species. The ion fluxes employed here are too low to affect the rate of hopping diffusion [14]. However, not all the adsorbate is in a mobile state at a given instant, since indium easily becomes immobilized by substitution into the top layer of Si(111) [18] and Ge(111) [21]. Ions can change the concentration of indium atoms in the mobile state by creating surface defects—either vacancies or In adatoms. Ions can create such species in several ways: (i) by pushing In atoms up into an adatom positions, (ii) by knock-in of In atoms into the bulk, with subsequent adatom formation by interstitial up-diffusion to the surface, and (iii) by formation of bulk Si interstitial-bulk vacancy pairs, with subsequent vacancy up-diffusion to the surface. In addition, Si adatoms formed by analogous surface or bulk processes can exchange with In atoms in the surface plane to form In adatoms. Such exchange has been observed for metals [26] and in molecular dynamics simulations of semiconductors [27].

Note that all these mechanisms involve modifying the number of surface defects, but in the third mechanism, those defects originate from ion-induced defect creation in the near-surface bulk. The defect formation process that operates in the present case is not known. However, what

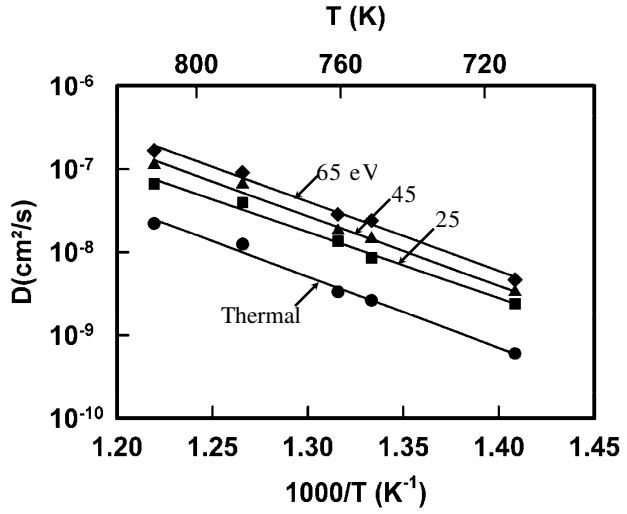

FIG. 2. Arrhenius plots for indium diffusion on Si(111) under Ar^+ bombardment at several energies. The lines represent linear fits using a constant E_{diff} of 1.65 eV.

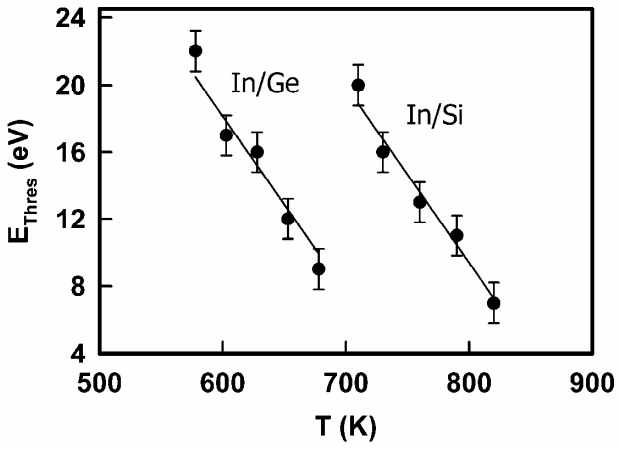

FIG. 3. Temperature dependence of E_{thres} for indium on Si and Ge. E_{thres} decreases linearly with T according to $E_{\text{thres}} = E_{\text{tot}} - \sigma kT$. The lines represent fits using $\sigma = 1320$ for both surfaces.

matters is that the energy threshold for one of the ion-enhanced defect formation processes should correspond to the threshold for ion-enhanced surface diffusion. Also, any temperature variation in the former threshold should be faithfully reproduced by a corresponding variation in the latter. These correspondences should hold regardless of the specific mechanism, since the simulations of Ref. [15] show the same behavior in all respects except the numerical values of E_{tot}. Thus, experimental results that confirm Eq. (1) give strong evidence for the existence of a broad class of temperature-dependent ion-induced defect formation processes.

The linear functional relationship between T and E_{thres} that is represented by Eq. (1) for surface diffusion mirrors that proposed in Ref. [15] for ion-induced point defect formation. The simulations yielded this same functional form for all types of surface and bulk point defects examined. Also, the experimental error ranges for σ on the two surfaces overlap, indicating that there is no observable difference in the strength of the temperature dependence for E_{thres}. Correspondingly, the simulations predicted essentially constant values of σ for defect creation involving Si and Ge substrates. The averaged value observed here of $\sigma = 1320$ for the two surfaces falls within a factor of 2 of the value of 700 observed in the simulations. With σ fixed at 1320 for the two surfaces, the fitted value of E_{tot} for Si in the experiments is larger by 12 eV than for Ge. The corresponding difference is about 25 eV in the simulations except for adatom formation, where the difference is 17 eV. In summary, the observed experimental results reproduce key qualitative predictions of the simulations, and despite the presence of a new atomic species (In), also reproduce the quantitative features within a factor of 2.

As discussed in connection with the simulations [15], temperature-dependent energy thresholds for defect formation result from a greatly enhanced probability of defect formation when target atoms on or within the substrate deviate substantially from their lattice sites due to thermal vibrations. At low temperatures, substrate atoms remain near their lattice sites, so that the net repulsive potential experienced by incoming ions is nearly uniform. Thus, the ions simply reflect off the surface with no defect creation. At higher temperatures, however, large-amplitude thermal vibrations degrade the uniformity. Ions that fortuitously impact asperities in the potential can wedge into them to create defects. As temperature increases, the number of highly displaced target atoms rises sharply, as does the number of defects formed.

This picture explains why the number of defects should increase with temperature for a constant ion energy. To explain why the threshold energy should depend upon temperature, however, requires an additional consideration. As ion energy decreases, the ions penetrate less closely to target atom cores. Less penetration makes the net repulsive potential at closest ion approach look more uniform as shown in Fig. 4. Thus, target atoms must make larger excursions from their lattice sites to permit defect formation. As temperature increases, target atoms make larger excursions, thereby permitting lower-energy ions that penetrate less closely to create defects.

Both experiments and simulations indicate that the magnitude of this temperature variation depends weakly upon the type of defect created and the identity of the substrate (at least for the diamond crystal structure). This insensitivity may result from two compensating factors connected with lattice stiffness. In stiff lattices with a steep repulsive potential between substrate atoms, the maximum excursions of target atoms are small and do not increase very rapidly with temperature. However, the repulsive potential between substrate atoms and incoming ions is also steep, so that ions of all energies penetrate fairly close to substrate atoms. Thus, only small excursions of substrate atoms are required to permit defect formation. Figure 4 sketches this situation for surface defect creation mechanisms. Bulk defects would obey a largely analogous picture. In less stiff lattices whose repulsive potential between atoms varies more slowly with distance, the maximum excursions of target atoms are comparatively large and also increase

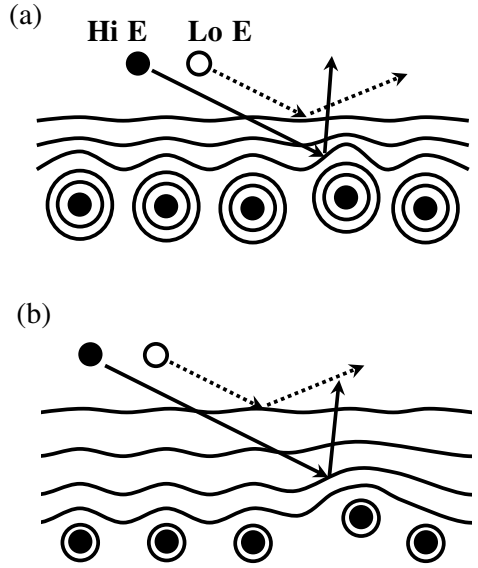

FIG. 4. Sketch illustrating why the rate of temperature variation of E_{thres} remains the same for different substrate materials. Contours of constant repulsive potential are shown schematically for stiff (a) and less stiff (b) lattices, together with typical ion trajectories for ions above and below E_{thres}. Near E_{thres}, defects are produced when ions hit asperities in the potential, and the ions reflect in nonspecular directions. (a) For stiff lattices with a steep repulsive potential, thermal vibrations cause small substrate atom excursions that vary slowly with temperature, but only small excursions are needed for ions to induce defects. (b) For less stiff lattices, the thermal excursions are larger and vary more rapidly with temperature but are compensated by the need for larger excursions to produce defects because low-energy ions penetrate less closely.

more rapidly with temperature. However, the repulsive potential experienced by ions varies correspondingly slowly with distance, so that the distance of closest approach varies more strongly with ion energy. Ions with lower energies remain further from substrate atoms than for stiff lattices, and target atoms must make larger excursions from lattice sites before defects can form. Thus, the larger rate of excursion increase with temperature is largely compensated by the larger excursions required. Note that this argument does not depend on the precise type of defect formed and therefore applies equally well to adatom formation, knock-in, sputtering, or bulk defect formation. Also note that E_{tot} does not have a simple physical interpretation (such as a thermodynamic defect formation energy), since only a small fraction of the incident ion energy is deposited into the target atom. Also, other factors enter in such as the angle of incidence of the ions and their azimuthal angle around crystallographic symmetry axes.

The effects described here could be exploited in a variety of applications. For example, in the ion implantation of dopants for semiconductor devices, the final stages of ion deceleration determine the dynamics of defect formation near the *pn* junction [28,29]. Changing temperature during implantation could controllably modulate such effects, as some literature suggests [4–6]. Moreover, the mechanism outlined here is not specific to group IV semiconductors and may characterize low-energy ion interactions with crystalline materials quite generally. In applications such as ion beam-assisted deposition and reactive ion etching, the net behavior often represents a delicate balance among various elementary rates. For example, enhanced surface diffusion in ion beam-assisted deposition typically improves materials properties, whereas concurrent defect formation, substrate sputtering, and embedding of the bombarding gas typically lead to degradation [24]. It may therefore be possible to exploit the threshold effects described here by judicious tuning of temperature and ion energy to select for specific defect formation or sputtering processes.

This work was partially supported by NSF (CTS 98-06329 and CTS 02-03237).

*Corresponding author.
Electonic address: eseebaue@uiuc.edu

[1] J. Wong-Leung, C. Jagadish, M. J. Conway, and J. D. F. Gerald, J. Appl. Phys. **89**, 2556 (2001).
[2] K. Tsujimoto, S. Okudaira, and S. Tachi, Jpn. J. Appl. Phys., Part 1 **30**, 3319 (1991).
[3] J. A. Gregus, M. F. Vernon, R. A. Gottscho, G. R. Scheller, W. S. Hobson, R. L. Opila, and E. Yoon, Plasma Chem. Plasma Process. **13**, 521 (1993).
[4] N. Nitta, M. Taniwaki, T. Suzuki, Y. Hayashi, Y. Satoh, and T. Yoshiie, Mater. Trans. **43**, 674 (2002).
[5] B. A. Turkot, D. V. Forbes, I. M. Robertson, J. J. Coleman, L. E. Rehn, M. A. Kirk, and P. M. Baldo, J. Appl. Phys. **78**, 97 (1995).
[6] K. Shoji, A. Fukami, T. Nagano, T. Tokuyama, and C. Y. Yang, Appl. Phys. Lett. **60**, 451 (1992).
[7] M. Nastasi, J. W. Mayer, and J. K. Hirvonen, *Ion-Solid Interactions: Fundamentals and Applications* (Cambridge University Press, New York, 1996).
[8] B. W. Dodson, Nucl. Instrum. Methods Phys. Res., Sect. B **59/60**, 481 (1991).
[9] A. Kuronen, J. Tarus, and K. Nordlund, Nucl. Instrum. Methods Phys. Res., Sect. B **153**, 209 (1999).
[10] J. W. Rabalais, A. H. Al-Bayati, K. J. Boyd, D. Marton, J. Kulik, Z. Zhang, and W. K. Chu, Phys. Rev. B **53**, 10 781 (1996).
[11] S. M. Lee, C. J. Fell, D. Marton, and J. W. Rabalais, J. Appl. Phys. **83**, 5217 (1998).
[12] D. Marton, K. J. Boyd, and J. W. Rabalais, J. Vac. Sci. Technol. A **16**, 1321 (1998).
[13] R. Ditchfield and E. G. Seebauer, Phys. Rev. Lett. **82**, 1185 (1999).
[14] R. Ditchfield and E. G. Seebauer, Phys. Rev. B **63**, 125317 (2001).
[15] Z. Wang and E. G. Seebauer, Phys. Rev. B **66**, 205409 (2002).
[16] K. A. Schultz and E. G. Seebauer, J. Chem. Phys. **97**, 6958 (1992).
[17] K. A. Schultz, I. I. Suni, and E. G. Seebauer, J. Opt. Soc. Am. B **10**, 546 (1993).
[18] C. E. Allen, R. Ditchfield, and E. G. Seebauer, J. Vac. Sci. Technol. A **14**, 22 (1996).
[19] R. Ditchfield, D. Llera-Rodríguez, and E. G. Seebauer, Phys. Rev. Lett. **81**, 1259 (1998).
[20] R. Ditchfield, D. Llera-Rodríguez, and E. G. Seebauer, Phys. Rev. B **61**, 13 710 (2000).
[21] I. I. Suni and E. G. Seebauer, J. Chem. Phys. **100**, 6772 (1994).
[22] C. Steinbruchel, Appl. Phys. Lett. **55**, 1960 (1989).
[23] J. P. Chang, A. P. Mahorowala, and H. H. Sawin, J. Vac. Sci. Technol. A **16**, 217 (1998).
[24] J. E. Greene and S. A. Barnett, J. Vac. Sci. Technol. **21**, 285 (1982).
[25] P. Sigmund, in *Sputtering by Particle Bombardment I* (Springer-Verlag, New York, 1981), p. 9; M. Nastasi, J. W. Mayer, and J. K. Hirvonen, *Ion-Solid Interactions: Fundamentals and Applications* (Cambridge University Press, New York, 1996).
[26] G. L. Kellogg, Surf. Sci. Rep. **21**, 1 (1994).
[27] C. E. Allen, R. Ditchfield, and E. G. Seebauer, Phys. Rev. B **55**, 13 304 (1997).
[28] H. H. Lin, S. L. Cheng, L. J. Chen, C. Chen, and K. N. Tu, Appl. Phys. Lett. **79**, 3971 (2001).
[29] E. G. Roth, O. W. Holland, V. C. Venezia, and B. Nielson, J. Electron. Mater. **26**, 1349 (1997).